Environ. Sci. Technol. **1999**, *33,* 1116−1126

Formal Uncertainty Analysis of a Lagrangian Photochemical Air Pollution Model

MICHELLE S. BERGIN,[†] GREGORY S. NOBLET,[‡] KEVIN PETRINI,[†] JOYEL R. DHIEUX,[†,§] JANA B. MILFORD,*[,†] AND ROBERT A. HARLEY[‡]

University of Colorado, Department of Mechanical Engineering, Boulder, Colorado 80309, and University of California, Department of Civil and Environmental Engineering, Berkeley, California 94720

This study applied Monte Carlo analysis with Latin hypercube sampling to evaluate the effects of uncertainty in air parcel trajectory paths, emissions, rate constants, deposition affinities, mixing heights, and atmospheric stability on predictions from a vertically resolved photochemical trajectory model. Uncertainties in concentrations of ozone and other secondary compounds and in predicted changes due to 25% reductions in motor vehicle non-methane organic compound (NMOC) and nitrogen oxide (NO_x) emissions were examined. Surface wind measurements were interpolated over the modeling domain, and uncertainties were quantified using data withholding. The resulting wind fields and uncertainties were used to generate ensembles of trajectories ending at four Southern California air quality monitoring sites. A motor vehicle emissions inventory and associated uncertainties were derived from remote sensing and fuel sales data. Uncertainties in chemical rate parameters were obtained from expert reviews. Estimated uncertainties in O_3 range across the four sites from 24% to 57% (1 standard deviation (1σ) relative to the mean). Seven variables contribute almost 80% of this uncertainty. Reductions in motor vehicle NMOC reduce O_3 from $10 \pm 10\%$ (1σ) to $28 \pm 10\%$. With reductions in motor vehicle (NO_x) emissions, the change in O_3 ranges from an increase of $14 \pm 14\%$ to a decrease of $6.6 \pm 6.2\%$.

1. Introduction

While significant steps have been taken to reduce urban ozone, concentrations in many cities still regularly exceed the National Ambient Air Quality Standard (NAAQS). Because O_3 is a secondary pollutant, areas in violation of the NAAQS must utilize photochemical air quality models to estimate the effects of the emissions control strategies they propose for achieving compliance. Air quality models (*1*) are used to calculate pollutant concentrations, accounting for emissions, transport, chemistry, and deposition. These models require a large amount of input data and numerous assumptions, many of which affect predictions of control strategy responses. Quantification of uncertainties in modeling results is thus critical for improving air quality prediction methods and identifying effective management strategies.

Methods for quantifying the sensitivity of air quality model results to uncertainties in model parameters are well-established. The most widely used approach is parametric analysis, in which the outputs of a base case are compared to outputs from additional simulations with one parameter value changed at a time (*2*, *3*). This approach is valuable when the number of parameters of interest is limited. However, systematic sensitivity analysis techniques, including local techniques, such as the direct decoupled method (*4*) and Green's function methods (*5*), and global techniques, such as the Fourier amplitude sensitivity test (*6*), represent more efficient means of calculating sensitivities to large numbers of parameters. These systematic methods have been used primarily to study atmospheric chemistry in box model simulations (*7*−*9*), but in a few cases have been applied to three-dimensional (3-D) models (*10*, *11*).

Beyond sensitivity analysis, calculations in which probability distributions are propagated through the model to estimate uncertainties in output concentrations have been performed using Monte Carlo techniques for descriptions of gas-phase tropospheric chemistry (*12*−*14*). Monte Carlo analysis has also been used to propagate uncertainties through a Gaussian plume model (*15*) and single-cell trajectory models of sulfur chemistry (*16*), nitrogen chemistry (*17*), and O_3 formation (*18*). A preliminary Monte Carlo uncertainty analysis has recently been performed for the Urban Airshed Model (*19*). The study presented here extends the evaluation of uncertainties in photochemical air quality models by utilizing a systematic approach not restricted to local sensitivity analysis and by considering a more comprehensive set of parameters with carefully estimated uncertainties.

This study applied Monte Carlo analysis with Latin hypercube sampling (LHS; *20*, *21*) to the vertically resolved trajectory version of the California/Carnegie Institute of Technology (CIT) air quality model (*22*, *23*). The study evaluated the effects of uncertainties in 51 model parameters on predicted concentrations of O_3 and other secondary compounds and on the peak O_3 response to 25% reductions in motor vehicle non-methane organic compound (NMOC) and NO_x emissions. Sensitivity analysis was used to help select the parameters included in the Monte Carlo analysis. Multivariate linear regression analysis was applied to the Monte Carlo results to identify the parameters contributing the most uncertainty to selected model outputs.

2. Modeling and Uncertainty Analysis Methods

2.1. Model and Input Data Description. The trajectory version of the CIT air quality model (*24*) was selected for this study because of greater computational tractability than 3-D models and greater physical detail than the single-cell models to which uncertainty analysis has most often been applied. The trajectory model, which follows a parcel of air as it traverses an airshed, is based on the Lagrangian formulation of the atmospheric diffusion equation:

$$\frac{\partial C_i}{\partial t} = \frac{\partial}{\partial z}\left(K_{zz}\frac{\partial C_i}{\partial z}\right) + R_i(\underline{C}) \quad i = 1, ..., N \qquad (1)$$

where C_i is the ensemble mean concentration of species i, K_{zz} is the turbulent eddy diffusivity in the vertical direction, z, and $R_i(\underline{C})$ is the net rate of generation of species i by chemical reactions. The initial condition is $C_i(z,0) = C_i^0(z)$,

* Corresponding author e-mail: milford@colorado.edu; phone: (303)492-5542; Fax: (303)492−2863.
† University of Colorado.
‡ University of California.
§ Current address: U.S. Environmental Protection Agency, Region 8, 999 18th St., Suite 500, Denver, CO 80202.

10.1021/es980749y CCC: $18.00
Published on Web 02/25/1999

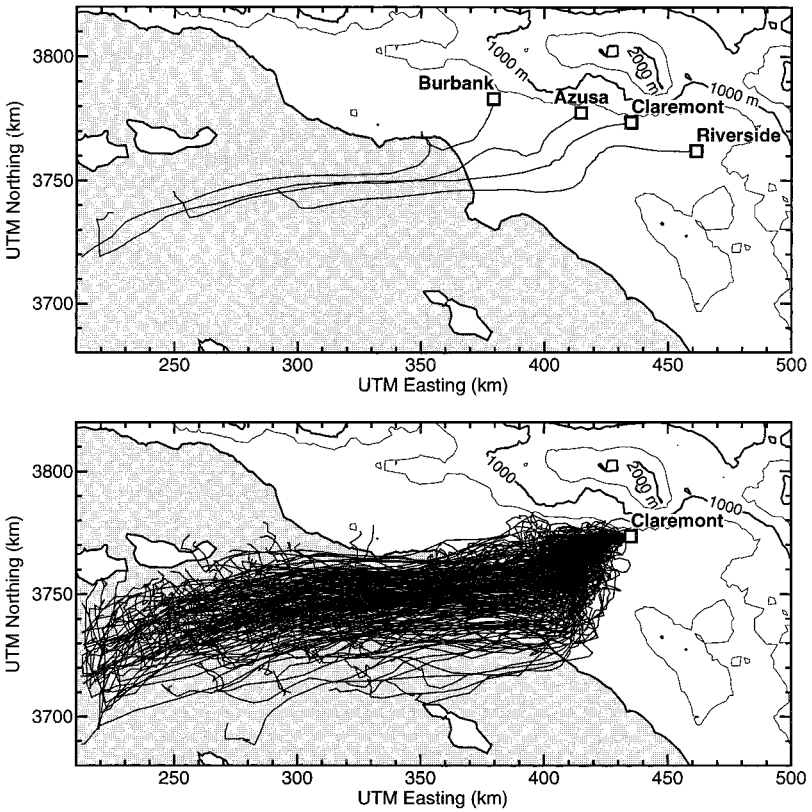

FIGURE 1. Nominal air parcel trajectories arriving at four receptor sites at hours of peak observed ozone concentrations (a, top). Nominal trajectories reach land on day 1 at 4:30 p.m. (Claremont), 6:30 p.m. (Azusa), 2:30 p.m. (Riverside), and 9:10 p.m. (Burbank). Ensemble of 200 uncertain air parcel trajectories arriving at Claremont at hour of peak observed ozone concentration (b, bottom). Topographic contours shown at 500 m intervals.

and the boundary conditions are

$$v_g^i C_i - K_{zz}\, \partial C_i/\partial z = E_i \quad \text{at the surface}$$

$$K_{zz}\, \partial C_i/\partial z = 0 \quad \text{at the top of the column}$$

Here, v_g^i is the surface deposition velocity and E_i is the surface emissions flux of species *i*. The most significant limitations of the trajectory formulation are its inability to account for horizontal diffusion and wind shear. The trajectory column modeled in this study is comprised of five vertical layers, matching the vertical structure used in the 3-D version of the CIT model (*25*, *26*).

The August 27−28, 1987, SCAQS episode in the South Coast Air Basin (SoCAB) provides one of the most comprehensive and well-evaluated urban air quality data sets available (*27*). Four SCAQS monitoring sites: Azusa, Burbank, Claremont, and Riverside, were selected as trajectory endpoints for analysis in this study. Observed peak O_3 concentrations range from 170 to 286 ppb at these four sites. Two-day trajectories were developed by back-calculating the paths of the air parcels starting from their arrival at each site at the time when peak O_3 concentrations were observed (Figure 1a).

The chemical mechanism and nominal rate parameter values used for this study were those of SAPRC93 (*28*) with 186 reactions and 83 species. Primary NMOC emissions are assigned to 11 lumped classes and 19 explicit species, as listed in Table 1 of Harley et al. (*26*). Photolysis rates were calculated using Peterson's (*29*) actinic flux estimates.

Initial conditions for air parcels originating over the Pacific Ocean were specified from concentrations measured during SCAQS at San Nicolas Island, CA, which is located about 110 km southwest of the Los Angeles area coastline. Main et al. (*30*) identified a "clean" profile of NMOC concentrations on days when insignificant recirculation of pollutants in the sea breeze−land breeze cycle was observed at San Nicolas Island. From that analysis, the initial conditions used in this study were 1 ppb NO, 1 ppb NO_2, 40 ppb O_3, 100 ppbC NMOC, and 200 ppb CO.

Emissions were input to the trajectory model in three separate source categories: on-road motor vehicle, biogenic, and "other" (stationary and off-road mobile) emissions. All emissions were input to the trajectory model at the surface. This is reasonable given the dominance of mobile and diffuse area source emissions in the SoCAB. As discussed below, on-road motor vehicle emissions were estimated from fuel sales, infrared remote sensing, and ambient pollutant concentration ratios. Estimates of stationary source and off-road mobile source emissions were developed by the California Air Resources Board and the South Coast Air Quality Management District. Biogenic emissions are based on the estimates developed by Causley and Wilson (*31*), which were used in previous studies (*25*, *26*). However, correction factors of 1.6 for isoprene and 1.3 for monoterpenes were applied in the current study. The correction factors reflect recent estimates by Benjamin et al. (*32*), who incorporated more finely resolved land-use data, updated emissions and environmental correction factors, and improved temperature fields.

Estimates of on-road motor vehicle emissions were developed using a fuel-based approach (*26*). Vehicle activity was measured by the amount of fuel consumed, and emission factors were normalized to fuel consumption. On-road measurements of CO emissions from more than 70 000 vehicles were made in summer 1991 (*33*) using infrared remote sensing at seven different Southern California monitoring sites. Remote sensing results were combined with fuel consumption data to estimate CO emissions (*34*). The

1991 estimates were scaled up to represent the older fleet on the road in 1987. Ambient pollutant concentration ratios were then used to estimate emissions of NO_x and NMOC (*26*).

The resulting SoCAB domain emissions of CO, NMOC, and NO_x used for this study are 8900×10^3, 2950×10^3, and 1150×10^3 kg day^{-1}, respectively. On-road motor vehicle emissions comprise 91%, 61%, and 62% of the total CO, NMOC, and NO_x emissions. The revised NMOC and NO_x emissions estimates are, respectively, 2.4 and 1.0 times the estimates of California's current official motor vehicle emission inventory model (MVEI 7G). Biogenic emissions contribute 6% of the total NMOC.

Deterministic surface wind fields were generated using meteorological data collected during the SCAQS at more than 60 monitoring sites (*27*). At most sites, surface wind speed and direction were measured continuously at a standard instrument height of 10 m; measured wind vectors were summed to calculate 1-h average resultant wind vectors. A three-step hybrid objective/diagnostic procedure (*35, 36*) was employed to construct 1-h average gridded surface wind fields from the measured wind data. First, *u* (westerly) and *v* (southerly) wind vector components were calculated at each grid square as weighted averages of the measured *u* and *v* vector components at the monitoring sites. The mountain ranges surrounding the Los Angeles air basin were treated as interpolation barriers. Second, the calculated *u* and *v* fields were refined to incorporate the effects of topography. Perturbations to the surface wind field due to variations in topography were calculated following the procedure described by Anderson (*37*). The final step in the generation of deterministic wind fields was the application of a five-point averaging filter to smooth the wind fields and reduce divergence. Further details on development of the wind fields are given by Noblet et al. (*38*).

2.2. Uncertainty in Model Parameters. The parameters that were treated as random variables in the uncertainty analysis and their coefficients of variation are presented in Table 1. Unless noted otherwise, the parameter uncertainties were treated as independent log-normally distributed variables with a mean of 1.0, sampled using LHS and applied as multiplicative factors to the nominal input or parameter values. Log-normal distributions are commonly assumed for physical variables that cannot have negative values. In addition to the variables discussed below, preliminary sensitivity calculations were also conducted to test the influence of variations in temperature, relative humidity, and the initial concentrations of O_3, NMOC, and NO_x. These parameters were found to have negligible impact and therefore were not included in the Monte Carlo analysis. Other potential sources of uncertainty that were neglected include the spatial and temporal distribution of emissions, and wind flows aloft. The expected significance of these omissions is discussed in section 5.

Wind Fields and Trajectory Paths. Uncertainty in the calculated wind fields was evaluated using the data-withholding technique described by McNair et al. (*46*). Measured wind data at a monitoring site were withheld from the data set, and the wind field was calculated as described above using the remaining data. The predicted *u* and *v* wind vector components at the grid square containing the withheld monitoring site were compared to the measured data at that site:

$$s_k = p_{ij} - o_k \qquad (2)$$

where s_k is the residual *u* or *v* wind vector component at monitoring site *k*; p_{ij} is the predicted *u* or *v* wind vector component at grid square *i,j*; and o_k is the measured *u* or *v* wind vector component at monitoring site *k*. The data-withholding analysis was repeated for each of 25 sites in a subset of the wind-monitoring network; the 25 sites are located near the trajectories of air parcels arriving at the selected SCAQS receptor sites (*38*).

Average *u* and *v* residuals across the 25 monitoring sites were calculated for each hour of the 2-day modeling period. Analysis of these results suggested grouping the residual data into separate sets for daytime and nighttime, with data from both days of the modeling period grouped together. During daytime hours (7 a.m. to 8 p.m.) the residual *u* and *v* data are normally distributed with mean values of $\sim$0 m s^{-1} and standard deviations of 0.83 and 0.64 m s^{-1}, respectively. Daytime average *u* and *v* wind speeds across the 25 sites are $+2.09$ and $+0.68$ m s^{-1}. During nighttime hours, the residual *u* and *v* data are normally distributed with mean values of $\sim$0 and standard deviations of 0.43 and 0.35 m s^{-1}, respectively. Nighttime average *u* and *v* wind speeds are $+0.35$ and -0.04 m s^{-1}. The residuals are not spatially correlated, but are serially correlated. The autocorrelation coefficients are $+0.50$ for *u* and $+0.49$ for *v* during the daytime, and $+0.33$ for *u* and $+0.21$ for *v* during the nighttime.

Ensembles of *n* air parcel trajectories with common end time and location were then calculated by adding stochastic *u* and *v* values, representing the uncertainty, to the deterministic *u* and *v* wind fields at each hour. The uncertainties in the *u* and *v* components were represented by normal distributions with mean, standard deviation, and autocorrelation values equal to those calculated from the residual data. LHS was used to construct *n* samples of stochastic *u* and *v* values for each hour of the 2-day modeling period. The stochastic values were sampled from the appropriate day or night distribution, depending on the hour. At each time step of the *n*th trajectory calculation, the stochastic *u* and *v* values from the appropriate hour of the *n*th sample were added to the *u* and *v* values from the deterministic wind field to determine the movement of the air parcel over that time step.

As an example, the ensemble of 200 air parcel trajectories computed for the Claremont receptor site is shown in Figure 1b. Across an ensemble, different air parcel paths result in different inputs to the model for spatially and temporally distributed variables such as emissions, temperature, and mixing height. In addition, differences in wind speed and mixing height affect the deposition velocities and vertical diffusivities calculated in the trajectory model. The trajectories begin at midnight on August 27, or when the back trajectory reaches the boundary of the modeling domain, and end on the afternoon of August 28 at the hour of the highest recorded O_3 concentration at each site. The "nominal" air parcel trajectory (Figure 1a) was also calculated for each site, using the deterministic wind fields only.

Emissions. The main uncertainty estimated for on-road motor vehicle emissions originates from site-to-site variability in remote sensing measurements of vehicle emissions in Southern California. On the basis of these data, 1σ uncertainties of $\pm$20% in CO emissions from cars and $\pm$30% for trucks (*34*) were found. The uncertainty in CO emissions also applies to NMOC and NO_x emissions from motor vehicles, because they are estimated from ambient concentration ratios to CO. This "general motor vehicle emissions" uncertainty was consequently treated as a multiplicative factor applied to CO, NMOC, and NO_x, and is log-normally distributed with a mean value of 1.0 and standard deviation of 0.25. Additional uncertainties in motor vehicle NMOC and NO_x emissions arise from the regression of ambient concentrations of NMOC and NO_x versus CO (*26*). These uncertainties were represented using two independent log-normally distributed random variables, referred to as "motor vehicle NO_x" and "motor vehicle NMOC", each with a mean of 1.0 and a standard deviation of 0.06.

TABLE 1. Distributions of Random Variables Included in Monte Carlo Analysis[a]

parameter label	description	COV[b] (ref)
	Air Parcel Trajectory	
CO_traj	sum of CO emissions in each trajectory	site dependent
	Claremont	0.116
	Azusa	0.122
	Riverside	0.146
	Burbank	0.233
	Pollutant Emissions	
MV_emis	motor vehicle general emissions (applied to CO, NO_x, and NMOC)	0.246 (*26, 34*)
MV_NO_x	motor vehicle NO_x (applied to NO_x only)	0.06 (*26*)
MV_NMOC	motor vehicle NMOC (applied to NMOC only)	0.06 (*26*)
Othr_NO_x	other anthropogenic NO_x	0.149
Othr_NMOC	other anthropogenic NMOC	0.294
Biog_emis	biogenic hydrocarbons: α-pinene, isoprene, higher lumped alkenes (OLE3)	0.385 (*32*)
	Chemistry: Reaction Rate Constants[c]	
$NO+O_3$	$NO + O_3 \rightarrow NO_2 + O_2$	0.095 (*39*)
$O(1D)+H_2O$	$O(^1D). + H_2O \rightarrow 2OH.$	0.183 (*39*)
O(1D)+M	$O(^1D). + M \rightarrow O(^3P). + M$	0.183 (*39*)
CO+OH	$CO + OH. \rightarrow HO_2. + CO_2$	0.265 (*40*)
HO_2+NO	$HO_2. + NO \rightarrow OH. + NO_2$	0.183 (*40*)
RCO3+NO[d]	RCO3. + NO → NO	0.343 (*39*)
RCO3+NO_2[e,f]	$RCO3. + NO_2 \rightarrow NO_2$	0.150 (*39, 41*)
RO2R+NO[g]	$RO_2R. + NO \rightarrow NO_2 + HO_2.$	0.417 (*39, 42*)
RCHO+*hν*	RCHO + *hν*_→ CCHO + RO2R. +RO2. + CO + HO_2.	0.343 (*42*)
PPN	PPN → C2CO−O2. + NO2 + RCO3	0.804 (*43, 44*)
ALK2+OH	[lumped alkanes] + OH. → products	0.265 (*42*)
ARO2+OH	[lumped aromatics] + OH. → products	0.265 (*42*)
OLE2+OH	[lumped alkenes] + OH. → products	0.183 (*42*)
$OLE2+O_3$	[lumped alkenes] + O_3 → products	0.417 (*42*)
$NO_2+h\nu$	$NO_2 + h\nu \rightarrow NO + O(^3P).$	0.183 (*39*)
$O_3+h\nu$	$O_3 + h\nu \rightarrow O(^1D). + O_2$	0.265 (*39*)
AFG2+*hν*[h]	[aromatic fragmentation products] + *hν* → products	1.333 (*42*)
HCHO+*hν*[i]	$HCHO + h\nu \rightarrow 2HO_2. + CO$	0.343 (*39*)
NO_2+OH[f]	$NO_2 + OH. \rightarrow HNO_3$	0.265 (*40*)
ETHE+OH[f]	ETHE + OH. → RO2R. + RO2. + 1.56HCHO + 0.22CCHO	0.114 (*39*)
PAN	PAN → CCO−O_2. + NO_2 + RCO3.	0.385 (*43, 44*)
	Mixing Heights	
MH_xxxx	mixing height for period ending at time xxxx; 11 periods are represented, from 0 to 2400 min.	see text
	Deposition[j]	
O_3_aff	O_3 deposition affinity	0.29
NO_aff	NO deposition affinity	0.29
NO_2_aff	NO_2 deposition affinity	0.29
	Atmospheric Stability	
Pas_Gif[k]	Pasquill−Gifford classification	0.11

[a] Distributions are independent and log-normal with a mean of 1.0 unless noted otherwise. [b] Coefficient of Variation (COV) = standard deviation normalized by nominal value at 298 K and 1 atm. [c] A complete listing of the mechanism and species definitions is given by Carter (*28, 45*). [d] Correlated ($\rho = 1$) with rate constants for CCO−O_2. + NO → CO_2 + NO_2 + HCHO + RO2R. + RO2.; C2COO2. + NO → CO_2 + NO_2 + CCHO + RO2R. + RO2.; and for other peroxyacyl radical reactions with NO (*45*). [e] Correlated ($\rho = 1$) with rate constants for CCO−O_2. + NO_2 → PAN; C2COO2. + NO_2 → PPN; and rate constants for other peroxyacyl radical reactions with NO_2 (*45*). [f] Coefficient of variation calculated from Troe parameter uncertainty estimates (*13*). [g] Correlated ($\rho = 1$) with rate constants for R2O2 + NO → NO_2; RO2 + NO → NO; and for other peroxy radical reactions with NO (*45*). [h] Correlated ($\rho = 1$) with rate constant for AFG1 + *hν* → HO_2. + HCOCO−O_2. + RCO3. [i] Correlated ($\rho = 1$) with rate constant for HCHO + *hν* → H_2 + CO. [j] Deposition affinity distributions are assumed to be uniform. [k] The Pasquill−Gifford distributions are discrete and are described in detail in the text.

Uncertainties in NO_x and NMOC emissions from other anthropogenic sources were treated as independent, log-normally distributed random variables, with means of 1.0 and standard deviations of 0.15 for NO_x and 0.30 for NMOC. For both NMOC and NO_x, this category of emissions is approximately equally split in the SoCAB between point sources and area sources (including off-road mobile sources). The standard deviations used in the uncertainty analysis were calculated by propagation of errors from subjectively estimated 1σ uncertainties of 10% and 25% for point and area sources of NO_x and 20% and 50% for point and area sources of NMOC. The uncertainty in the biogenic emissions estimates was treated as a log-normally distributed multiplicative factor with a mean of 1.0 and standard deviation of 0.4. The standard deviation was obtained by assuming that the range of recent estimates cited by Benjamin et al. (*32*) corresponds to $\pm 1\sigma$ bounds.

Chemical Parameters. Rate parameters of 29 reactions, listed in Table 1, were treated as random variables in the Monte Carlo calculations. Uncertainties in product yields were not considered because previous studies (*47, 14*) have shown that their quantifiable influence is relatively small. The set of uncertain rate parameters was identified in a two-stage screening process (*48*). In the first stage, the direct decoupled method (*4*) was applied to single-cell model simulations following eight trajectories in the SoCAB, to calculate the local sensitivity of O_3 concentrations to each of the rate constants in the SAPRC93 mechanism. Rate constant uncertainties were estimated as described by Yang et al. (*13*), from uncertainty factors given by review panels (*40, 49, 50*)

or original estimates (*42*) for parameters specific to the SAPRC mechanism. The sensitivity coefficients and rate parameter uncertainties were then combined to estimate how much each parameter contributes to uncertainty in the final O_3 concentrations.

The 50 rate parameters with average uncertainty contributions greater than 0.001% were treated as random variables in the second stage of the screening analysis. In this stage, Monte Carlo simulations were run for the eight trajectories with Latin hypercube samples of $n = 200$. Correlations between related rate parameters were incorporated in the sampling scheme. On the basis of this analysis, the rate parameters listed in Table 1 account for more than 95% of the total uncertainty due to chemical parameters in the final predicted O_3 concentrations. After completion of the screening analysis, uncertainty estimates for some of the rate parameters were updated on the basis of the evaluation by DeMore et al. (*39*).

Mixing Height. The mixing height values used in the trajectory model were inferred from vertical profiles of potential temperature derived from rawinsonde measurements (*25*). Six soundings per day were obtained at eight sites covering the coastal and inland regions of the air basin. Two to three soundings per day were available from several other sites. Mixing height estimates from the soundings were spatially and temporally interpolated to cover the modeling region and simulation period.

Estimation of mixing heights from potential temperature profiles is somewhat subjective. For example, for the August 27−28 episode, the discrepancies in estimates from different members of our group interpreting the same profiles ranged from 0 to about 80 m (*51*). Moreover, the precision to which the height can be specified is limited to about 25 m by the resolution at which the sounding data are reported. Spatial and temporal interpolation of the estimated mixing heights introduces further uncertainty. Overall, these factors are judged to produce 1σ uncertainties in the mixing height estimates of 10% between 10 a.m. and 4 p.m. and 20% between 4 p.m. and 10 a.m. A separate random variable was used to represent the uncertainty for the time interval between each of the six daily soundings. The vertical diffusivity in the trajectory model depends on the mixing height and so is affected by this uncertainty.

Deposition Affinities. The trajectory version of the CIT model calculates an upper limit value for the dry deposition velocity based on local surface roughness and meteorological conditions and then multiplies this value by a species-specific "deposition affinity" ranging from 0 to 1, to account for removal at less than the transport-limited rate. This treatment of dry deposition has been replaced with a surface resistance scheme in the 3-D version of the CIT model (*25*). For the trajectory model, deposition affinities for individual species and meteorological variables governing vertical eddy diffusivities are significant sources of uncertainty in the dry deposition calculations. Preliminary sensitivity calculations were used to determine that deposition affinities for O_3, NO, and NO_2 needed to be included as random variables in the Monte Carlo calculations. For the other species, either the deposition affinity was already set to 1 (e.g., for HNO_3) or increasing the deposition affinity by 50% produced less than a 1% change in the final O_3 concentrations. The deposition affinities for O_3, NO, and NO_2 were subjectively assigned uniform, independent probability distributions spanning the range from 0.5 to 1.5 times their nominal values.

Stability Class. Deposition velocities and vertical diffusivities in the trajectory model depend on the Monin−Obukhov length, which is calculated through a correlation based on the Pasquill−Gifford stability class. The stability class assignment is determined from surface wind speed measurements and solar radiation estimates (*52*). Uncertainty was introduced into the stability parametrization through the wind speed, as described above, and through the assignment of the stability class. In the trajectory model, the stability classes are represented by values from 1 (unstable) to 6 (stable). A subjective, discretely distributed random error, ϵ, was added to the numerical assignments with a 50% probability that $\epsilon = 0$ and 25% probabilities that $\epsilon = -0.5$ or $+0.5$. Stability class values less than 1 or greater than 6 were precluded. A single sample value of ϵ was incorporated for the whole simulation period, since it represents uncertainty in the classification scheme. In tests with ϵ as the only random variable in the trajectory model, the resulting standard deviation in the vertical diffusivity ranged from about 10% to 30%, depending on time and cell height.

2.3. Uncertainty Propagation and Regression Analysis. The influence of input parameter uncertainties on the CIT trajectory model predictions was evaluated through Monte Carlo simulations followed by multivariate linear regression analysis. For each trajectory endpoint, a set of model simulations was conducted in which one member of the ensemble of trajectory paths was matched with a value of each of the other random inputs drawn from the assigned distributions using LHS. LHS is a stratified sampling technique in which values are drawn from randomly matched "bins" of equal probability. This technique ensures that the full range of each distribution is represented with a minimal sample size requirement.

The main model outputs of interest for this study are the final hour concentrations of O_3, HNO_3, HCHO, PAN, and reactive nitrogen (NO_y). NO_y is calculated here as the sum of NO, NO_2, HNO_3, and PAN concentrations, accounting for more than 93% of total NO_y. Using the Monte Carlo outputs, the influence of each parameter on a final hour concentration is estimated using the linear regression equation

$$C_{ij} = \beta_{i0} = \sum_q \left(\beta_{iq} \frac{P_{qj}}{P_q} \right) \tag{3}$$

where C_{ij} = the predicted value of interest for output i from simulation j, β_{i0} = the regression intercept, β_{iq} = the regression coefficient of the influence of parameter q on output i, P_{qj} = the value of parameter q from simulation j, and P_q = the nominal value for parameter q.

Regression coefficients were found by minimizing the squared residuals between the values of C_{ij} obtained from each simulation and the value predicted by eq 3. Residuals from the multivariate regression model were examined and found to be approximately normally distributed, with constant variance. Coefficient of determination (R^2) values indicating the proportion of variance explained by the multivariate linear regression model are given with the regression results presented below.

To solve the regression equations, values for P_{qj} and P_q must be defined for each input parameter. This is generally straightforward. However, variation in the trajectory path incorporates potential differences in wind speed and direction, emissions, temperature, mixing height, and other variables. After evaluating a number of options by using them in the regression analysis and comparing the resulting R^2 values for the Claremont endpoint, the normalized sum of CO emissions along the trajectories was selected as best able to represent the variation due to the trajectory path. The variation in CO emissions for each of the four ensembles of trajectories is given in Table 1. Considering only the variations due to the trajectory paths, correlation of total NMOC emissions with CO emissions ranged from 0.93 for Azusa to 0.99 for Burbank. NO_x and CO emissions correlations ranged from 0.68 for Azusa to 0.93 for Burbank.

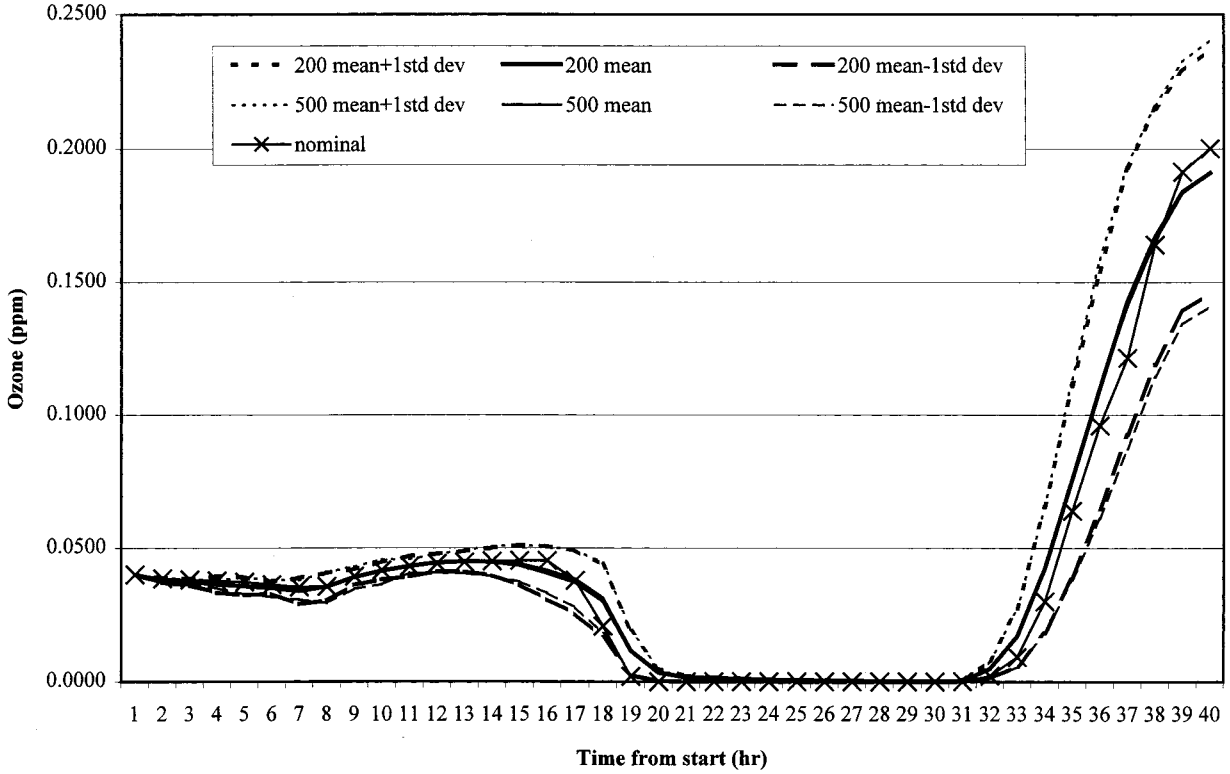

FIGURE 2. Sample size convergence of Monte Carlo results for ozone at Claremont.

The regression coefficients from eq 3 are used to calculate the contributions of the parameters to the uncertainties in the outputs from

$$UC_{iq} = \frac{COV_q^2 \beta_{iq}^2}{\sigma_i^2} \times 100 \qquad (4)$$

where UC_{iq} = the percent contribution of the uncertainty in parameter q to the uncertainty in output i, COV_q = the coefficient of variation for parameter q, and σ_i = the standard deviation of output i from the Monte Carlo simulations.

To evaluate uncertainties in control scenarios, each Latin hypercube sample was used in paired simulations of a base case and a control case. Two control cases were examined for each site: the base case simulations were repeated with a 25% reduction in motor vehicle NO_x emissions and with a 25% reduction in motor vehicle NMOC emissions. The output variable in eqs 3 and 4 was then defined as the percent reduction in predicted peak O_3 between the paired simulations of the base and control cases.

3. Evaluation of Uncertainty Propagation and Regression Analysis Methods

Detailed evaluation of the uncertainty propagation and regression methods was conducted primarily for a trajectory path ending at the Claremont monitoring site at 2:30 p.m. on August 28, 1987, when the observed O_3 concentration was 0.286 ppm. Claremont is downwind of the Los Angeles central urban area and often has high O_3 concentrations. The model simulation for the Claremont trajectory using nominal parameter values results in a final O_3 concentration of 0.200 ppm, 30% lower than the point observation. This site was used to evaluate the effect of sample size on the convergence of output means, standard deviations, and regression results.

First, an appropriate number of sample values, n, must be determined. A large enough sample size must be used so that selected statistics converge and spurious correlation between variables is avoided, while a minimum sample size is desired to control the computational requirements of the simulations. To select the sample size for this study, simulations were run using LHS sample sizes of n = 100, 150, 200, 250, and 500 values per parameter. As discussed below, a sample size of 200 was chosen. Consequently, the sample size comparison presented here is limited to the sets with n = 200 and 500.

Figure 2 compares the mean and standard deviation in O_3 concentrations along the Claremont trajectory, calculated from Monte Carlo simulations with LHS sample sizes of n = 200 and 500. These statistics are very similar throughout the simulation for the two sample sizes. The mean final O_3 concentration with both sample sizes is 0.191 ppm, slightly lower than the nominal concentration of 0.200 ppm. The standard deviation is 0.047 ppm for n = 200, and 0.052 for n = 500. The observed O_3 concentration, 0.286 ppm, is two standard deviations above the mean value from the Monte Carlo simulations. The means and standard deviations of the other secondary pollutant concentrations predicted from the two sample sets converged similarly.

Table 2 shows the uncertainty contribution and the percent change in regression coefficients for the parameters that contribute more than 1% to the uncertainty in the final O_3 concentration. The largest source of uncertainty is motor vehicle emissions. Other influential parameters include the rate constants for the reactions NO_2+OH, RCO3+NO, NO_2+$h\nu$, and PAN decomposition; the trajectory path (represented by cumulative CO emissions); and the O_3 deposition affinity. The average percent difference in the regression coefficients calculated with n = 200 versus 500 is 20%. This degree of error associated with a sample size of n = 200 was judged to be acceptable for this application, given the trade-off in added computational requirements with a larger sample size.

Beyond the issue of choosing an adequate sample size, a potentially more fundamental limitation of the regression

TABLE 2. Comparison of Regression Coefficients from Sample Sizes of $n = 200$ versus 500 for Parameters Contributing to Uncertainty in Ozone at Claremont

parameter	UC (%)[a]	$\Delta\beta_q$[b] (%)
MV_emis	22.5	5.7
NO_2+OH	9.3	3.6
RCO3+NO	9.0	−42
CO_traj	8.9	−0.7
$NO_2+h\nu$	7.8	20
O_3_aff	4.6	29
PAN	3.7	−1.7
RCO3+NO_2	3.4	−36
PPN	1.7	4.9
NO+O_3	1.7	−53
AFG2+$h\nu$	1.5	−26

[a] UC = uncertainty contribution from $n = 200$ sample set for parameters contributing more than 1% of the total uncertainty. [b] $\Delta\beta_q$ = change in regression coefficient for parameter $q = ((\beta_{q,n=500} - \beta_{q,n=200})/\beta_{q,n=500}) \times 100\%$.

TABLE 3. Comparison of Observed and Modeled Ozone Concentrations (ppm) for Four Trajectory Endpoint Sites

		Claremont	Azusa	Riverside	Burbank
observed		0.286	0.240	0.240	0.170
trajectory model	nominal	0.200	0.167	0.246	0.213
Monte Carlo ($n = 200$)	mean	0.191	0.185	0.185	0.161
Monte Carlo ($n = 200$)	COV (%)[a]	24.6	34.8	24.0	57.3

[a] COV = (standard deviation/mean) × 100%.

analysis method is the possibility that relationships between the output variables and some uncertain parameters are nonlinear. To examine this possibility, scatter plots of O_3 at Claremont versus about 20 input variables and plots of O_3 versus emissions at all four sites were examined. With a few minor deviations, the scatter plots appeared either linear or uncorrelated.

4. Comparison of Uncertainty Results across Trajectory Endpoints

4.1. Ozone Uncertainty. Predicted final O_3 concentrations from the uncertainty analysis are presented for all four sites in Table 3. The coefficients of variation for O_3 concentrations range from 24% at Riverside to 57% at Burbank. The mean final O_3 concentrations are within 1σ of the observed values at Azusa and Burbank and within 2σ at Riverside and Claremont. The final concentration from the nominal simulations is within 1σ of the mean concentration at all sites except Riverside, where it is within 2σ. The mean concentration is higher than the nominal value at Azusa, but lower than the nominal values at the other three sites. For all sites, the observed O_3 concentrations, which are point measurements, are consistently higher than the predicted mean values, which represent volume averages.

The Burbank endpoint has the highest uncertainty in O_3 and the largest variation in emissions, as indicated by the coefficient of variation for CO emissions shown in Table 1. Burbank is located in the northwest corner of the air basin, in an area with complex surrounding topography and wind fields. The nominal trajectory approaches from the southwest (Figure 1a); the ensemble of 200 uncertain trajectories is distributed to either side of it. Trajectories lying southeast of the nominal path pass over areas with relatively high emissions. In contrast, those lying northwest of it pass near the Santa Monica Mountains, where emissions are relatively low. Additionally, of the four trajectory ensembles, those ending at Burbank spend the least mean time over land, 15.3 h. The mean time spent over land for the other trajectory ensembles is 19.8 h for those ending at Azusa, 22.3 h for Claremont, and 23.4 h for Riverside. Correspondingly, the variance in emissions for each of these ensembles is lower than for the Burbank ensemble.

Table 4 presents the regression coefficients and uncertainty contributions to final O_3 concentrations for 11 parameters contributing the most uncertainty at each site. The R^2 values for the regression range from 0.76 at Azusa to 0.82 at Riverside. A total of 15 parameters are listed, among which seven contribute about 80% of the identified uncertainty for all of the sites.

The most influential parameters are very similar for all four sites. Motor vehicle general emissions are the largest source of uncertainty at three of the four locations and the second largest source of uncertainty at the fourth, Burbank. The trajectory path is the largest source of uncertainty in the O_3 concentration at Burbank and is among the top four most influential factors at the other sites. Modeled O_3 concentrations at all four sites are also sensitive to chemical parameters, including rate constants for HNO_3 formation, RCO3+NO, NO_2 photolysis, and PAN decomposition. Uncertainty in the O_3 deposition affinity is also influential at Claremont, Azusa, and Riverside. Of note, the complete set of regression coefficients (not shown) indicates that O_3 concentrations at Azusa, Burbank, and Claremont are highly sensitive to the independent variation of motor vehicle NMOC emissions and that concentrations at all four sites are sensitive to the independent variation in motor vehicle NO_x emissions. These parameters do not show up in Table 4 because their estimated uncertainties are small.

Because the trajectory path is influential, but cannot be directly represented in the regression analysis, the effect of its uncertainty on O_3 concentrations was determined in

TABLE 4. Regression Coefficients (ppm) and Uncertainty Contributions (%) of Parameters Contributing the Most Uncertainty in Ozone Concentrations

Claremont ($R^2 = 0.79$)			Azusa ($R^2 = 0.76$)			Riverside ($R^2 = 0.82$)			Burbank ($R^2 = 0.80$)		
	β	UC		β	UC		β	UC		β	UC
MV_emis	0.091	22.5	MV_emis	0.114	19.0	MV_emis	0.070	14.9	CO_traj	0.261	43.2
NO_2+OH	−0.054	9.3	CO_traj	0.183	12.0	CO_traj	0.115	14.4	MV_emis	0.107	8.0
RCO3+NO	0.041	9.0	NO_2+OH	−0.077	10.0	$NO_2+h\nu$	0.072	8.9	RCO3+NO	0.048	3.2
CO_traj	0.121	8.9	RCO3+NO	0.050	7.0	RCO3+NO	0.031	5.8	$NO_2+h\nu$	0.083	2.7
$NO_2+h\nu$	0.072	7.8	$NO_2+h\nu$	0.089	6.3	O_3_aff	−0.035	5.3	MH_2040	−0.074	2.6
O_3_aff	−0.035	4.6	AFG2+$h\nu$	0.010	4.0	NO_2+OH	−0.037	5.0	NO_2+OH	−0.055	2.5
PAN	0.023	3.7	PAN	0.027	2.6	PAN	0.019	2.8	O_3_aff	−0.040	1.6
RCO3+NO_2	−0.058	3.4	O_3_aff	−0.035	2.5	NO+O_3	−0.070	2.3	PAN	0.029	1.5
PPN	0.008	1.7	RCO3+NO_2	−0.062	2.1	NO_2_aff	−0.022	2.0	RCO3+NO_2	−0.072	1.4
NO+O_3	−0.065	1.7	Othr_NMOC	0.024	1.2	PPN	0.007	1.7	AFG2+$h\nu$	0.008	1.3
AFG2+$h\nu$	0.004	1.5	HCHO+$h\nu$	0.020	1.1	MH_2040	0.024	1.1	HCHO+$h\nu$	0.029	1.1

TABLE 5. Secondary Pollutant Concentrations (ppm) from Nominal and Monte Carlo Simulations

		Claremont	Azusa	Riverside	Burbank
HCHO	nominal	0.0235	0.0272	0.0275	0.0312
	mean	0.0249	0.0267	0.0227	0.0287
	COV (%)	27.7	33.3	30.0	49.5
HNO_3	nominal	0.0166	0.0251	0.0267	0.0204
	mean	0.0149	0.0175	0.0149	0.0170
	COV	39.6	40.0	36.9	63.5
PAN	nominal	0.0075	0.0068	0.0083	0.0123
	mean	0.0075	0.0088	0.0056	0.0090
	COV	45.3	54.5	51.8	82.2
NO_y	measured (NO_x)	0.0760	0.1000	0.0300	0.0700
	nominal	0.0441	0.0816	0.0512	0.0800
	mean	0.0448	0.0619	0.0344	0.0825
	COV	29.9	31.7	29.7	39.4

isolation. Simulations were performed using the trajectory model for ensembles of 100 trajectories ending at each location, with all other inputs and parameters set to their nominal values (*38*). The resulting final O_3 concentrations were 0.207 ± 0.024, 0.201 ± 0.030, 0.197 ± 0.027, and 0.176 ± 0.082 ppm at Claremont, Azusa, Riverside, and Burbank, respectively. These results indicate that the trajectory path uncertainty is the source of the bias between the mean and nominal values at Riverside. The results also underscore the large uncertainty due to the trajectory path at Burbank.

On the basis of the results of the data-withholding analysis applied to the wind field interpolation procedure, serial correlations of up to +0.50 were incorporated into the trajectory path uncertainties. To test the importance of the correlations, final O_3 concentrations at Claremont were compared for samples of 100 trajectories generated with and without autocorrelation in the wind field uncertainties (again with no other uncertainties considered). With wind field uncertainties treated as independent from 1 h to the next, the final O_3 concentration from the Monte Carlo analysis is 0.207 ± 0.020 ppm. Thus, the autocorrelation increases the uncertainty in the output O_3 concentration, due to the tendency for deviations from the nominal trajectory to accumulate over time.

4.3. Uncertainty in Other Secondary Species. Monte Carlo results for HCHO, HNO_3, PAN, and NO_y are presented in Table 5. The uncertainties in their final concentrations are consistently highest at Burbank, and lowest at Claremont and Riverside. Uncertainties in HCHO concentrations are comparable to those for O_3, ranging from 28% to 50%. Uncertainties in HNO_3 concentrations range from 37% at Riverside to 64% at Burbank. PAN concentrations exhibit the highest uncertainties, ranging from 45% at Claremont to 82% at Burbank. Uncertainties in NO_y concentrations are relatively consistent across sites, ranging from 30% to 40%. Mean concentration predictions tend to be lower than the nominal predictions, with the maximum percent difference being 44% for HNO_3 at Riverside. Approximate NO_x concentrations were measured at these sites using chemiluminescent analyzers and are shown for comparison with NO_y concentration predictions. The trajectory model did not consistently over- or underpredict NO_y concentrations in comparison to the NO_x measurements, and the mean NO_y concentration is predicted to within 15−41% of the measured NO_x.

Table 6 presents regression results for HCHO, HNO_3, PAN, and NO_y concentrations for the three parameters that contribute most of the uncertainty at each site. R^2 values range from 0.53 for HNO_3 at Claremont to 0.93 for HCHO at the same site. The highest R^2 value is always found for HCHO and the lowest for HNO_3. In addition to motor vehicle emissions and trajectory paths, HCHO photolysis rate constants are highly influential for HCHO concentrations. Motor vehicle emissions, the NO_2 deposition affinity, and the rate constant for HNO_3 formation are the largest sources of uncertainty in HNO_3 concentrations, except at Burbank, where the trajectory path is most influential. As with O_3, motor vehicle emissions are the largest source of uncertainty in PAN concentrations at Azusa, Claremont, and Riverside, with the trajectory path contributing the largest share at Burbank. Finally, motor vehicle emissions, other NO_x emissions, the trajectory path, and the NO_2 deposition affinity control the uncertainty in NO_y at all four sites. As expected, uncertainties in chemical parameters have relatively little influence on NO_y.

4.4. Uncertainty in Emissions Control Cases. The influence of input and parameter uncertainties was also examined for responses to 25% reductions in motor vehicle NO_x and NMOC emissions. The results are shown in Figure 3. For the case studied, O_3 concentrations at Burbank and Azusa appear

TABLE 6. Regression Coefficients (ppm) and Uncertainty Contributions (%) of Parameters Contributing the Most Uncertainity in Secondary Pollutant Concentrations

Claremont			Azusa			Riverside			Burbank		
	β	UC		β	UC		β	UC		β	UC
HCHO											
	($R^2 = 0.93$)			($R^2 = 0.85$)			($R^2 = 0.92$)			($R^2 = 0.87$)	
MV_emis	0.018	40.7	MV_emis	0.021	33.7	MV_emis	0.015	28.7	CO_traj	0.038	38.4
HCHO+$h\nu$	−0.010	22.3	HCHO+$h\nu$	−0.010	15.2	CO_traj	0.023	24.1	MV_emis	0.024	16.7
CO_traj	0.022	14.2	CO_traj	0.023	9.6	HCHO+$h\nu$	−0.009	21.5	HCHO+$h\nu$	−0.010	5.5
HNO_3											
	($R^2 = 0.53$)			($R^2 = 0.62$)			($R^2 = 0.63$)			($R^2 = 0.69$)	
MV_emis	0.0090	14.1	MV_emis	0.0127	19.9	MV_emis	0.0085	14.5	CO_traj	0.0280	36.6
NO_2_aff	−0.0064	9.9	NO_2_aff	−0.0065	7.3	NO_2_aff	−0.0047	6.1	MV_emis	0.0151	11.8
NO_2+OH	0.0054	5.9	NO_2+OH	0.0056	4.5	NO_2+OH	0.0051	6.0	Othr_NO_x	0.0148	4.2
PAN											
	($R^2 = 0.83$)			($R^2 = 0.80$)			($R^2 = 0.83$)			($R^2 = 0.77$)	
MV_emis	0.0076	30.2	MV_emis	0.0103	27.9	MV_emis	0.0055	21.8	CO_traj	0.0214	45.5
PAN	−0.0038	18.5	CO_traj	0.0161	16.7	PAN	−0.0035	21.6	MV_emis	0.0103	11.7
CO_traj	0.0096	10.7	NO_2+OH	−0.0055	9.2	CO_traj	0.0073	13.6	MH_2040	−0.0067	3.3
NO_y											
	($R^2 = 0.62$)			($R^2 = 0.63$)			($R^2 = 0.76$)			($R^2 = 0.70$)	
MV_emis	0.027	24.4	MV_emis	0.037	21.4	MV_emis	0.024	33.8	CO_traj	0.072	26.4
NO_2_aff	−0.017	13.1	NO_2_aff	−0.028	16.9	NO_2_aff	−0.010	7.8	MV_emis	0.058	19.1
MV_NO_x	0.050	5.1	Othr_NO_x	0.033	6.4	MV_NO_x	0.040	5.5	Othr_NO_x	0.060	7.7

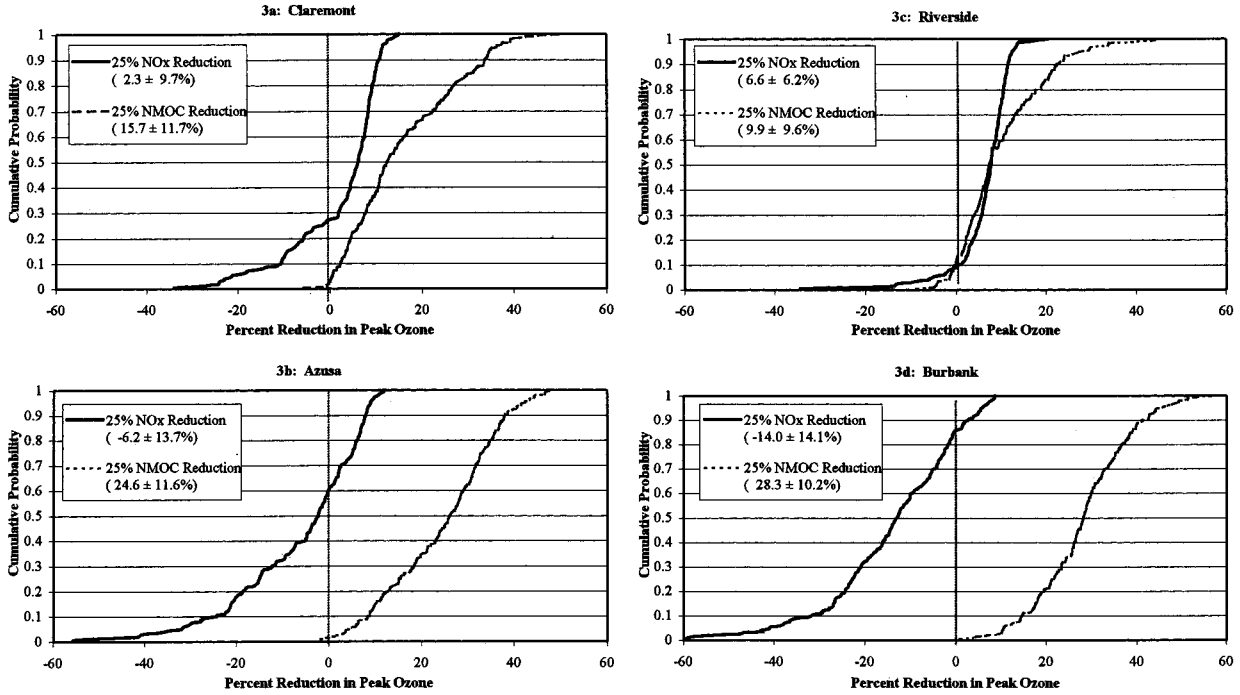

FIGURE 3. Cumulative probability of percentage reductions in peak O_3 due to a 25% decrease in motor vehicle NO_x or NMOC emissions at (a) Claremont, (b) Azusa, (c) Riverside, and (d) Burbank. Mean $\pm$ 1σ shown in legends.

TABLE 7. Regression Coefficients (%) and Uncertainty Contributions (%) of Parameters Contributing the Most Uncertainty to Percent Reduction in Ozone from 25% Reductions in Motor Vehicle NO_x and NMOC Emissions

NMOC Control

Claremont ($R^2 = 0.65$)			Azusa ($R^2 = 0.62$)			Riverside ($R^2 = 0.52$)			Burbank ($R^2 = 0.62$)		
	β	UC		β	UC		β	UC		β	UC
NO_2+OH	17.1	14.8	NO_2+OH	19.0	19.0	NO_2+OH	14.0	15.1	NO_2+OH	15.9	16.9
NO_2_aff	−13.1	10.5	NO_2_aff	−12.3	9.5	AFG2+$h\nu$	−2.2	9.4	MV_emis	10.5	6.3
CO_traj	−31.5	9.7	CO_traj	−24.6	6.7	MV_NO_x	33.3	4.4	AFG2+$h\nu$	−1.6	4.4
AFG2+$h\nu$	−2.5	8.3	HCHO+$h\nu$	−6.3	3.5	RCO3+NO	−5.3	3.6	Othr_NMOC	−7.0	4.0
HCHO+$h\nu$	−6.5	3.6	MH_2040	10.5	3.3	CO_traj	−11.3	3.0	MV_NO_x	33.5	3.9
MV_NO_x	37.1	3.6	MV_NO_x	33.6	3.0	Othr_NO_x	10.6	2.7	Othr_NO_x	13.2	3.7

NO_x Control

Claremont (R^2 =0.62)			Azusa ($R^2 = 0.59$)			Riverside ($R^2 = 0.41$)			Burbank (R^2 =0.63)		
	β	UC		β	UC		β	UC		β	UC
NO_2+OH	−12.0	10.7	NO_2+OH	−20.7	16.0	RCO3+NO	4.7	6.7	NO_2+OH	−18.8	12.6
CO_traj	27.0	10.3	CO_traj	35.7	10.1	CO_traj	10.8	6.6	AFG2+$h\nu$	3.4	10.6
AFG2+$h\nu$	2.2	9.1	NO_2_aff	14.7	9.7	AFG2+$h\nu$	1.2	6.2	CO_traj	18.4	9.4
NO_2_aff	9.3	7.6	AFG2+$h\nu$	2.5	6.0	NO_2+OH	−5.1	4.8	MV_NMOC	54.8	5.5
RCO3+NO	6.5	5.2	MH_2040	−13.4	3.9	Othr_NO_x	−6.9	2.8	MV_NO_x	−54.1	5.3
MV_emis	6.8	2.9	HCHO+$h\nu$	5.3	1.7	NO_2_aff	3.1	2.2	NO_2_aff	9.0	3.5

[a] Mean and standard deviation of percent reduction in peak ozone.

to be robustly NMOC-limited. Reducing NMOC emissions by 25% along the Burbank trajectory is estimated to reduce O_3 by 28 $\pm$ 10%. The result for Azusa is a reduction of 25 $\pm$ 12%. In both cases, the best estimate of the effect of reducing NO_x emissions is an increase in O_3, although the percentage change is highly uncertain. For Riverside and Claremont, the mean reductions in O_3 are higher with a 25% decrease in NMOC emissions than with a 25% decrease in NO_x emissions. At Riverside, however, the median (50th percentile) results of both strategies are equal. At all of the sites, uncertainties in the NO_x control results indicate that peak O_3 could increase or decrease with 25% reductions in motor vehicle NO_x emissions. The probability that the NO_x reductions will increase O_3 ranges from less than 10% at Riverside to about 85% at Burbank.

Regression results for the percent change in O_3 due to NMOC or NO_x reductions are shown in Table 7. Uncertainties in rate constants and other parameters that strongly affect the balance between NO_x and radicals along each trajectory appear most influential for the percent change in O_3 under both emissions reduction scenarios. Key among these are the rate constant for HNO_3 formation, the photolysis rate of unknown aromatic oxidation products (AFG2), and the NO_2 deposition affinity. The effects of NMOC reductions versus NO_x reductions show sensitivities to these parameters that are comparable in magnitude but opposite in sign.

The trajectory path also contributes significant uncertainty to the effect of NMOC and NO_x reductions. Increased CO emissions and the correlated increases in NO_x and NMOC emissions across trajectories are associated with an increase

in the effectiveness of NO_x reductions and a decrease in the effectiveness of NMOC reductions, except at Burbank, where they are associated with increases in the effectiveness of both strategies.

Except at Burbank, responses to NO_x or NMOC emission reductions are much less sensitive to the general uncertainty in motor vehicle emissions than are absolute O_3 concentrations. However, other emission uncertainties are more influential for the responses to emission reductions than for absolute concentrations. For example, the independent uncertainty in motor vehicle NO_x emissions contributed from 3.0% (Azusa) to 4.4% (Riverside) of the uncertainty in O_3 responses to motor vehicle NMOC emission reductions. The independent uncertainty in motor vehicle NMOC emissions contributes 5.5% of the uncertainty in the response to NO_x reductions at Burbank.

5. Discussion

For four trajectory endpoints in the SoCAB, uncertainties in 51 input parameters of the CIT trajectory model resulted in 1σ uncertainties in final O_3 concentrations ranging from 24% to 57%. Uncertainties in predicted concentrations range from 28% to 50% for HCHO, 37% to 64% for HNO_3, 45% to 82% for PAN, and 30% to 40% for NO_y. Except at one site, Riverside, the finding that a 25% reduction in motor vehicle NMOC emissions reduces O_3 more than a 25% reduction in NO_x emissions is robust with respect to the uncertainties evaluated. Uncertainties in a small number of parameters, including the trajectory path, motor vehicle emissions, and a few chemical parameters, are highly influential for all of the model outputs.

Some of the findings of this study may be unique to the SoCAB trajectories selected for analysis. In particular, the influence of trajectory path uncertainties is strongly affected by the emissions distribution in the SoCAB, which features sharp discontinuities in emissions at the coast and in the mountainous portions of the airshed. Compared to many other urban areas, the SoCAB is also unique in having a relatively small impact from transported pollutants and in having a relatively dense network of air quality and meteorological monitoring stations to provide model inputs. Although the quantitative results of this analysis cannot be generalized to other locations, the methods demonstrated here should be widely applicable.

The use of sensitivity analysis to guide the selection of random variables and Latin hypercube sampling to reduce Monte Carlo sample size requirements is an effective approach for evaluating the cumulative influence of uncertainties in large numbers of model inputs and parameters. In addition, regression analysis of the Monte Carlo results can provide useful estimates of how much uncertainty is contributed by individual input parameters.

The results of this study provide guidance for future uncertainty analyses of 3-D air quality models applied to the SoCAB. Previous studies have shown that changes in chemical parameters and emissions have a similar influence in trajectory and 3-D models (*3*). Although the influence of wind field uncertainties does not transfer directly, the findings of this study should also help guide the quantification of uncertainties in 3-D wind fields. In particular, it appears necessary to assess uncertainty in the *u* and *v* components of wind velocity separately and to consider that wind field uncertainty may vary with time of day.

The limitations of this study include the neglect of wind shear and horizontal diffusion, and the outdated deposition velocity parametrization used in the trajectory model. The model sensitivity to the O_3 deposition affinity suggests that updating the deposition velocity treatment could have a significant effect on the results. In addition, some potentially important input parameters were not considered in the present uncertainty analysis. These parameters include wind flows aloft, as discussed below, and the spatial and temporal distribution of emissions. The spatial and temporal distribution of diesel NO_x emissions is of particular concern, as it is known to be different from that of light-duty vehicle emissions (*53*).

The inability to represent wind shear and recirculation of air aloft is a fundamental limitation of the trajectory model. In the SoCAB, return flows aloft accompany onshore winds occurring near the surface. The effect of the offshore flow could be to increase regional background concentrations of O_3 and precursors over the ocean. However, O_3 levels in the highly polluted Los Angeles basin are most sensitive to emissions and meteorology within the well-mixed layer near the surface. For this highly polluted episode, the sensitivity of O_3 to initial conditions was small. Initial conditions and recirculation effects may be more important in future-year scenarios with large reductions in mainland emissions.

Uncertainty analysis results obviously depend on the estimates made for uncertainties in the inputs. A critical aspect of these estimates is appropriate treatment of correlations with other parameters. In this study, for example, because motor vehicle emissions of CO, NO_x, and NMOC were all estimated from remote sensing data for CO, the main source of uncertainty was common to all three pollutants. These joint uncertainties produce different results than would be obtained if large, independent uncertainties were assumed for each pollutant. In particular, this study found a relatively small effect of motor vehicle emission uncertainties on responses to emission reductions because the NO_x and NMOC emission variations were correlated. As shown above, autocorrelations in wind component uncertainties are also important.

Uncertainties in chemical rate parameters were obtained primarily from expert panel reviews, which are not always consistent across reviews and are often controversial. A particular problem arises with the rate parameters for the oxidation of aromatics, for which the reaction mechanism has not been established. These parameters are estimated by fitting the results of model predictions to measured O_3 concentrations in chamber experiments and thus depend on other parameter values used in the SAPRC mechanism. The estimated coefficient of variance for the AFG1 and AFG2 photolysis rates, 1.333 (*42*), is the largest used in this study and may be an overestimate. Detailed evaluation of uncertainties due to the chamber experiments and chemical mechanisms used to estimate these parameters could yield improved estimates of this value.

Previous sensitivity and uncertainty analyses of chemical parameters have also identified rate constants for aromatics oxidation, HNO_3 formation, NO_2 photolysis, and PAN formation and decomposition as highly influential for peak O_3 concentrations under polluted conditions (*14*) and for incremental reactivities of organic compounds (*2, 3, 13*). The uncertainty estimates for PAN, acetyl peroxy radical + NO_x, and NO_2 photolysis parameters used in this study are lower than estimates used in the earlier studies. The changes reflect updates to the SAPRC mechanism and a revised evaluation of confidence in the NO_2 action spectra.

Finally, uncertainty analysis results for changes in O_3 due to NMOC and NO_x emission reductions illustrate the importance of performing uncertainty analysis for control scenarios, as well as for absolute concentrations in historical episodes. Different parameters emerge as most influential in each case. For example, uncertainty in the rate constant for HNO_3 formation contributed most to the uncertainty in the predicted O_3 response to motor vehicle NO_x and NMOC emission reductions at three of the four sites, whereas the general uncertainty in motor vehicle emissions was most influential for base case O_3 concentrations. Uncertainties in

other emissions categories were more influential for O_3 control strategy evaluations than for base case O_3. These results should help set priorities for future research and model improvements. In addition, consideration must be given to designing control strategies that are robust with respect to variations in those parameters for which further reductions in uncertainty are not practical.

Acknowledgments

The authors would like to thank Dr. William P.L. Carter for assistance in using the SAPRC93 chemical mechanism. This work was funded by the U.S. Environmental Protection Agency, assistance agreement R 824797-01-0.

Literature Cited

(1) Seinfeld, J. H. *J. Air Poll. Control Assoc.* **1988**, *38* (5), 616−645.
(2) Bergin, M. S.; Russell, A. G.; Carter, W. P. L.; Croes, B. E.; Seinfeld, J. H. *VOC Reactivity and Urban Ozone Control, Encyclopedia of Environmental Analysis and Remediation;* John Wiley & Sons: New York, 1998; pp 3355−3383.
(3) Bergin, M. S.; Russell, A. G.; Milford, J. B. *Environ. Sci. Technol.* **1998**, *32*, 694−703.
(4) Dunker, A. M. *J. Chem. Phys.* **1984**, *81*, 2385−2393.
(5) Hwang, J. T.; Dougherty, E. P.; Rabitz, S.; Rabitz, H. *J. Chem. Phys.* **1978**, *69*, 1580−1591.
(6) Koda, M.; McRae, G. J.; Seinfeld, J. H. *Int. J. Chem. Kinet.* **1979**, *11*, 427−444.
(7) Falls, A. H.; McRae, G. J.; Seinfeld, J. H. *Int. J. Chem. Kinet.* **1979**, *CI*, 1137−1162.
(8) Pandis, S. N.; Seinfeld, J. H. *J. Geophys. Res.* **1989**, *94*, 1105−1126.
(9) Milford, J. B.; Gao, D. Russell, A. G.; McRae, G. J. *Environ. Sci. Technol.* **1992**, *26*, 1179−1189.
(10) Dunker, A. M. *Atmos. Environ.* **1981**, *15*, 1155−1161.
(11) Yang, Y.-J.; Wilkinson, J. G.; Russell, A. G. *Environ. Sci. Technol.* **1997**, *31*, 2859−2868.
(12) Thompson, A. M.; Stewart, R. W. *J. Geophys. Res.* **1991**, *96*, 13089−13108.
(13) Yang, Y.-J.; Stockwell, W. R.; Milford, J. B. *Environ. Sci. Technol.* **1995**, *29*, 1336−1345.
(14) Gao, D.; Stockwell, W. R. Milford, J. B. *J Geophys. Res.* **1996**, *101*, 9107−9119.
(15) Freeman, D.; Egami, T. T.; Robinson, N. F.; Watson, J. G. *J. Air Poll. Control Assoc.* **1986**, *36*, 246−253.
(16) Alcamo, J.; Bartnicki, J. *Atmos. Environ.* **1987**, *21*, 2121−2131.
(17) Derwent, R. G. *Atmos. Environ.* **1987**, *21*, 1445−1454.
(18) Derwent, R. G.; Hov, O. *J. Geophys. Res.* **1988**, *93*, 5185−5199.
(19) Hanna, S. R.; Chang, J. C.; Fernau, M. E. *Atmos. Environ.* **1998**, *32*, 3619−3628.
(20) Iman R. L.; Shortencarier, M. J. *A FORTRAN 77 Program and User's Guide for the Generation of Latin Hypercube and Random Samples for Use with Computer Models;* NUREG/CR-3624; Sandia National Laboratories: Albuquerque, NM, Mar 1984.
(21) Morgan, G. G.; Henrion, M. *Uncertainty: A Guide to Dealing with Uncertainty in Quantitative Risk and Policy Analysis*; Cambridge University Press: Boston, MA, 1990.
(22) Russell, A. G.; McRae, G. J.; Cass, G. R. *Atmos. Environ.* **1983**, *17*, 949−964.
(23) Pandis, S. N.; Harley, R. A.; Cass, G. R.; Seinfeld, J. H. *Atmos. Environ.* **1992**, *26A*, 2269−2282.
(24) McRae, G. J. and Russell, A. G. *Vertically resolved Lagrangian trajectory model;* Environmental Quality Laboratory, California Institute of Technology: Pasadena, CA, 1981.
(25) Harley, R. A.; Russell, A. G.; McRae, G. J.; Cass, G. R.; Seinfeld, J. H. *Environ. Sci. Technol.* **1993**, *27*, 378−388.
(26) Harley, R. A.; Sawyer, R. F.; Milford, J. B. *Environ. Sci. Technol.* **1997**, *31*, 2829−2839.
(27) Lawson, D. R. *J Air Waste Manag. Assoc.* **1990** *40*, 156−165.
(28) Carter, W. P. L. *Atmos. Environ.* **1995**, *29*, 2513−2527.
(29) Peterson, J. T. *Calculated Actinic Fluxes (290−700 nm) for Air Pollution Photochemistry Applications*; EPA-600/4−76−025; U.S. Environmental Protection Agency: Research Triangle Park, NC, 1976.
(30) Main, H. H.; Lurmann, F. W.; Roberts, P. T. *Pollutant concentrations along the western boundary of the South Coast Air Basin. Part I: a review of existing data;* Report to the South Coast Air Quality Management District; Sonoma Technology Inc.: Santa Rosa, CA, 1990.
(31) Causley, M. C.; Wilson, G. M. *Seasonal and annual average biogenic emission for the South Coast Air Basin generated by the SCAQMD biogenic database system;* Report to the South Coast Air Quality Management District; Systems Applications International: San Rafael, CA, 1991.
(32) Benjamin, M. T.; Sudol, M.; Vorsatz, D.; Winer, A. M. *Atmos. Environ.* **1997**, *31*, 3087−3100.
(33) Stedman, D. H.; Bishop, G. A.; Beaton, S. P.; Peterson, J. E.; Guenther, P. L.; McVey, I. F.; Zhang, Y. *On-road Remote Sensing of CO and HC Emissions in California;* Report to the California Air Resources Board; University of Denver: Denver, CO, 1994.
(34) Singer, B. C. and Harley, R. A. *J. Air Waste Manage. Assoc.* **1996**, *46*, 441−447.
(35) Goodin, W. R.; McRae, G. J.; Seinfeld, J. H. *J. Appl. Meteorol.* **1979**, *18*, 761−771.
(36) Goodin, W. R.; McRae, G. J.; Seinfeld, J. H. *J. Appl. Meteorol.* **1980**, *19*, 98−108.
(37) Anderson, G. E. *J. Appl. Meteorol.* **1971**, *10*, 377−386.
(38) Noblet, G.; Harley, R.; Dhieux, J.; Milford, J. *Effect of Wind Field Uncertainty on Predictions of a Lagrangian Photochemical Air Quality Model*, 98-RA76B.02, Proceedings of the 91st Annual Meeting of the Air & Waste Management Association, San Diego, CA, June 14−18, 1998.
(39) DeMore, W. B.; Golden, D. M.; Hampson, R. F.; Howard, C. J.; Ravishankara, A. R.; Kolb, M. J.; Molina, M. J. *Chemical Kinetics and Photochemical Data for Use in Stratospheric Modeling, Evaluation No. 12*, JPL Publication No. 97-4; Jet Propulsion Laboratory: Pasadena, CA, 1997.
(40) DeMore, W. B.; Sander, S. P.; Golden, D. M.; Hampson, R. F.; Kurylo, M. J.; Howard, C. J.; Ravishankara, A. R.; Kolb, M. J.; Molina, M. J. *Chemical Kinetics and Photochemical Data for Use in Stratospheric Modeling, Evaluation No. 11*; JPL Publication No. 94-26; Jet Propulsion Laboratory: Pasadena, CA, 1994.
(41) Bridier, I.; Caralp, F.; Loirat, H.; Lesclaux, R.; Veyret, B.; Becker, K. H.; Reimet, A.; Zabel, F. *J. Phys. Chem.* **1991**, *95*, 3594−3600.
(42) Stockwell, W. R.; Yang, Y.-J.; Milford, J. B. *A Compilation of Estimated Uncertainty Factors for Rate Constants in W. P. L. Carter's Detailed Mechanism*; Auto/Oil Air Quality Improvement Research Program, March 1994.
(43) Atkinson, R.; Baulch, D. L.; Cox, R. A.; Hampson, R. F.; Kerr, J. A.; Troe, J. *J. Phys. Chem. Ref. Data* **1992**, *21*, 919−1600.
(44) Grosjean, D.; Grosjean, E.; Williams II, E. L. *J. Air Waste Manage. Assoc.* **1994**, *44*, 391−396.
(45) Carter, W. P. L. *Atmos. Environ.* **1990**, *24A*, 481−518.
(46) McNair, L. A.; Harley, R. A.; Russell, A. G. *Atmos. Environ.* **1996**, *30*, 4291−4301.
(47) Yang, Y.-J.; Stockwell, W. R.; Milford, J. B. *Environ. Sci. Technol.* **1996**, *30*, 1392−1397.
(48) Petrini, K. *Uncertainty Analysis of an Atmospheric Regional-Scale Gas-Phase Chemical Mechanism*; M.S. Thesis, Department of Chemical Engineering, University of Colorado, Boulder, 1997.
(49) Atkinson, R.; Baulch, D. L.; Cox, R. A.; Hampson, R. F., Jr.; Kerr, J. A.; Troe, J. *J. Phys. Chem. Ref. Data* **1989**, *13*, 1259−1380.
(50) DeMore, W. B.; Sander, S. P.; Golden, D. M.; Molina, M. J.; Hampson, R. F.; Kurylo, M. J.; Howard, C. J.; Ravishankara, A. R. *Chemical Kinetics Data For Use In Stratospheric Modeling; Evaluation No. 9*; Jet Propulsion Laboratory: Pasadena, CA, 1990.
(51) Dhieux, J. *The Impact of Wind Field Uncertainty on Predictions of a Photochemical Trajectory Model Applied to the Los Angeles Basin*, M.S. Thesis, Department of Civil, Environmental and Architectural Engineering, University of Colorado, Boulder, 1997.
(52) Turner, D. B. *Workbook of Atmospheric Dispersion Estimates*, U.S. Environmental Protection Agency: Washington, DC, 1970.
(53) Dreher, D. B.; Harley, R. A. *J. Air Waste Manage. Assoc.* **1998**, *48*, 352−358.

Received for review July 22, 1998. Revised manuscript received January 4, 1999. Accepted January 28, 1999.

ES980749Y